determined by the upper limit in the series expansion. This new expression provides an accurate characterization of the CRLH-TL using a number of expansion terms much smaller than the number of unit cells in the physical lumped-element line. It can be used for reduced-order modeling of circuits that contain a large quantity of CRLH-TLs composed of many unit cells.

REFERENCES

1. C. Caloz, H. Okabe, T. Iwai, and T. Itoh, Transmission-line approach of left-handed (LH) materials, USNC/URSI Natl Radio Sci Mtg, San Antonio, TX, 2002, p. 39.
2. A.K. Iyer and G.V. Eleftheriades, Negative refractive index metamaterials supporting 2D waves, IEEE MTT Int Symp, Seattle, WA, 2002, pp. 1067–1070.
3. C. Caloz and T. Itoh, Transmission-line approach of left-handed (LH) structures and microstrip realization of a low-loss broadband LH filter, IEEE Trans Antennas Propagat (to appear).
4. A. Sanada, C. Caloz, and T. Itoh, Characteristics of the composite right/left-handed transmission lines, IEEE Microwave Wireless Compon Lett (to appear).
5. C. Caloz and T. Itoh, Novel microwave devices and structures based on the transmission-line approach of meta-materials, 2003 IEEE MTT-S Int Microwave Symp Dig 1 (2003), 195–198.
6. Y. Tanji and A. Ushida, Closed-form expression of RLCG transmission line and its application, IEICE Trans Fundamentals J86-A (2003), 739–748.
7. A. Escassut, Analytic elements in p-adic analysis, World Scientific, 1995.
8. R.E. Collin, Foundations for microwave engineering, 2nd ed., McGraw Hill, New York, 1992.

GUIDED-WAVE MICROLENS ARRAY APPLICATIONS TO COMPACT 1 × 8 PLANAR WAVEGUIDE SPLITTERS

Chun-Wen Chang and Wen-Feng Hsieh
Institute of Electro-Optical Engineering
National Chiao Tung University
Hsinchu, Taiwan 30050, ROC

Received 17 March 2004

ABSTRACT: *A compact 1 × 8 waveguide splitter using a guided-wave microlens array is presented and analyzed to show low insertion loss and output imbalance of 0.28 and 0.15 dB, respectively. The analysis results show that the proposed equal-power splitter with insensitive wavelength responses and acceptable fabrication tolerances is applicable for compact and wide-bandwidth integrated optical devices.* © 2004 Wiley Periodicals, Inc. Microwave Opt Technol Lett 43: 29–33, 2004; Published online in Wiley InterScience (www.interscience.wiley.com). DOI 10.1002/mop.20365

Key words: *waveguide splitter; guided-wave lens; optical waveguide; integrated optics*

1. INTRODUCTION

An optical power-splitter waveguide is one of the key components in fiber-optical communication systems. In the subscriber network of a passive optical network (PON), a power-splitter waveguide can be used to distribute optical power from one input channel into several output ones. Conventional $1 \times N$ power splitters are constructed by cascading Y-branch waveguides [1, 2]; the dimensions of the optical-power splitter become very large, as the number of output ports increases. Consequently, it is desirable to develop a new structure for compact, multibranch, planar power splitters.

Various types of multibranch power splitters have been demonstrated [3–10]. The 1×3 power splitter can be achieved by using a relatively low-index phase-front accelerator region in the Y-branch structure [3] or by disposing a couple of waveguide expanders and a microprism to tilt the phase front of the incident wave [4]. For the 1×4 waveguide power splitter, the multimode demultiplexing (MMD) waveguide power splitter was proposed to redistribute the power of the single-mode input to four single-mode outputs through a multimode section [6]. The multimode interference (MMI) [7–9] splitters are another attractive approach to design compact power splitters; nevertheless, their wavelength-dependent characteristics and their tight fabrication tolerances [10] limit their applications. Free-space-type integrated-optic $N \times N$ star couplers [11], constructed by locating a slab waveguide region between the fan-shaped input and output waveguide arrays, are useful to separate and combine optical power in optical networks.

In this paper, we design a compact 1×8 planar waveguide splitter by using a guided-wave microlens [12], which was constructed by disposing lens-shaped waveguide regions in planar lightwave circuits. The proposed structure is similar to the Galilean telescope, except that the objective is replaced by a microlens array. Or to put it another way, the structure is equivalent to eight sets of the lateral-shifted waveguide telescopes.

The beam propagation method (BPM) is used to calculate the transmission efficiency and optical-field distribution. Since the embedded guided-wave lenses use materials of higher refractive indices, the finite-difference time-domain (FDTD) method is employed to observe the reflection and the scattering occurring in the waveguide-lens boundaries. Furthermore, the fabrication issue regarding the radius deviations of the lenses is also investigated in order to evaluate the practicability of the proposed devices; the wavelength responses of the proposed devices are also shown in these analyses.

2. DESIGN METHOD

In Figure 1(a), a guided-wave micro-telescope composed of a diverging lens A and a converging lens B is used as a mode converter in an integrated-optics system [13]. Lens A with a negative focal length f_A serves as the beam expander of the device. This beam expander accelerates the phase front in the center portion of the input beam and transfers more power from the input beam to the outer region with an increasing spot size. After leaving the tapered region, the diverged optical beam is converged by lens B of focal length f_B, which serves as the collimator of the device. In order to yield a plane-wave beam after leaving the mode converter, the focal length of lens B should fulfill the Galilean condition $\Delta z = f_B - |f_A|$, where Δz represents the tapered length of the mode converter. As shown in this figure, if one laterally shifts the collimate lens by Δx, the resultant beam will be tilted by an angle θ.

The proposed 1×8 planar power splitter is achieved in accordance with this design concept by replacing lens B with a microlens array [see Fig. 1(b)], which has a focal length identical to that of lens B. Consequently, the combination of each lenslet of the microlens array with the beam expander constitutes a lateral-shifted guided-wave telescope.

We employed the transfer function method to calculate the propagation of the optical wave in this lateral-shifted telescope structure, and to predict the propagating angle of the outgoing beam. Under the paraxial and thin-lens approximations, the transfer function of the guided-wave telescope structure in Figure 1(a) can be expressed as

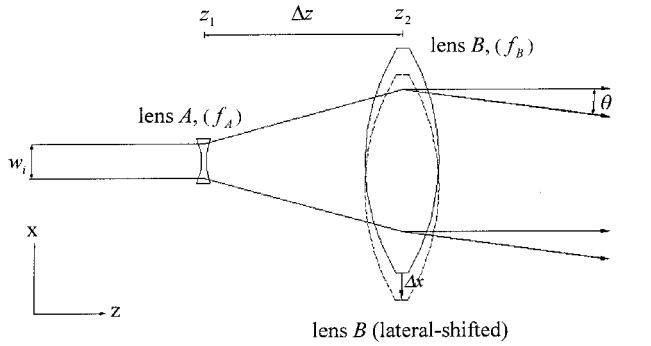

(a)

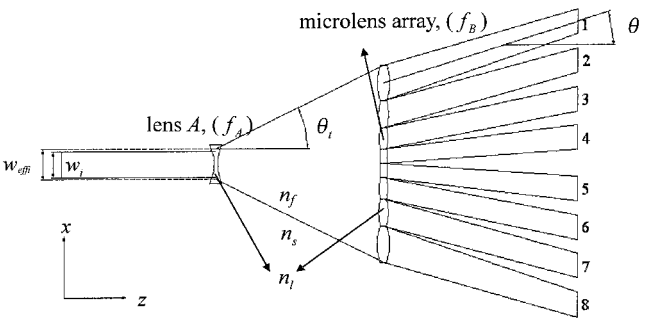

(b)

Figure 1 Schematics of (a) the mode converter constructed by using a conventional telescope structure and (b) the 1 × 8 equal-power splitter with input and output single-mode channels 1–8

$$\tilde{t}_A = \exp\left(+ j \frac{\pi x^2}{\lambda f_A}\right) \quad \text{and} \quad \tilde{t}_B = \exp\left(- j \frac{\pi (x - \Delta x)^2}{\lambda f_B}\right), \quad (1)$$

where $\tilde{t}_A$ describes the transmission function of lens A and $\tilde{t}_B$ is that of lens B, which is shifted laterally by Δx relative to lens A, and λ is the wavelength. The positive and the negative signs in the exponential of Eq. (1) are associated with diverging and converging lenses, respectively. Consider that a plane-wave beam with diameter w_i, as shown in Figure 1(a), is coaxial with lens A. After immediately leaving the first lens, the planar wavefront is altered by the refractive lens and the complex amplitude $\tilde{U}$ of the beam can therefore be described as

$$\tilde{U}(x, z = z_1^+) = E(x) \exp\left(j \frac{\pi x^2}{\lambda f_A}\right), \quad (2)$$

where $E(x)$ is the electric field distribution of the incident beam. The amplitude described by Eq. (2) represents a spherical wave that diverges from the focus of lens A. After traveling a distance Δz, that is, just in front of lens B, the beam diameter increases and the radius of curvature of the beam exactly matches the curvature of lens B. The complex amplitude is then given by

$$\tilde{U}(x, z = z_2^-) = E(x) \frac{f_A}{f_B} \exp\left(j \frac{\pi x^2}{\lambda f_B}\right). \quad (3)$$

Immediately behind lens B, the amplitude $\tilde{U}$ of the propagating wave is given by

$$\tilde{U}(x, z = z_2^+) = E(x) \frac{f_A}{f_B} \exp\left(- j \frac{\pi \Delta x^2}{\lambda f_B}\right) \exp\left(+ j \frac{2\pi \Delta x}{\lambda f_B} x\right). \quad (4)$$

The first phase term in Eq. (4) is constant and the second term, on the other hand, is far more interesting because it represents a linear phase shift across the aperture of the lens proportional to the lateral shift Δx. Consequently, the complex amplitude described in Eq. (4) reveals that the lateral-shifted telescope serves not only as a plane-wave beam shaping system, but also as a refractive prism that deflects the incoming plane-wave beam to an angle

$$\theta = + \arctan\left(\frac{\Delta x}{f_B}\right). \quad (5)$$

The positive sign in Eq. (5) indicates that the deflection takes place in the same direction as the lateral shift. Since the proposed lens set is equivalent to eight sets of lateral-shifted telescopes, the input beam will be split into eight collimated beams propagating at specific directions, as described by Eq. (5).

3. DEMONSTRATIONS OF NUMERICAL CALCULATION

The BPM is employed to calculate the normalized transmission power and optical field distribution of the proposed 1 × 8 planar power splitters shown in Figure 1(b). The geometrical and dielectric parameters of the input single-mode straight waveguide are: waveguide width $w_i = 9$ μm and refractive index $n_s = 1.5$, and $n_f = 1.504$ for the substrate and waveguide, respectively. It is assumed that the incident beam of wavelength $\lambda_0 = 1.5$ μm has the fundamental transverse electric (TE) mode. Using the above values, the effective width w_{effi} and the effective refractive index n_{eff} are calculated to be 14.04 μm and 1.503, respectively. Following the input waveguide, a laterally (one-dimensional) tapered waveguide with the tapered angle $\theta_t = 15°$ is used to connect the input waveguide to the eight output channels. In the proposed devices, the input end of the tapered region has a width of 9 μm and the width of output end is 72 μm.

The geometrical parameters of the beam expander and the microlens array can be determined from the Lensmaker's formula

$$\frac{n_m}{f} = (n_l - n_m)\left(\frac{1}{r_1} - \frac{1}{r_2}\right), \quad (6)$$

where f is the focal length of the lens, r_1 and r_2 are the radii of the curvatures of the lenses, and n_l and n_m are the refractive indices of the lens and the ambient medium, respectively. In Eq. (6), the radii of the curvatures are assumed to be the same on both sides of the lens and the effective refractive index n_{eff} of the straight waveguide is employed as n_m. The focal length can be determined if the tapered angle is specified; the thickness of the guided-wave lens, which did not affect the characteristic of the device significantly, is assumed to be 2 μm. In order to prevent excess loss from mode conversions, the effective widths w_{effi} of the straight waveguide are considered as the aperture of the beam expander in the proposed power splitters. In fabricating this device, the guided-wave lenses are patterned simultaneously with the channel waveguides in the same mask in order to eliminate the fabrication-tolerance issues. The material of the guided-wave lens set can be grown in a SiO_2/SiON material system, since the refractive index of SiO_2/SiON thin film can be adjusted over a large range, namely, between 1.45 (SiO_2) and 2.0 (Si_3N_4) [14]. Once we conveniently assume the refractive indices of all guided-wave lenses to be $n_l = 1.8$, the radii of the curvatures of these lenses can be determined as $r_A = 10.35$ μm and $r_B = 52.53$ μm for the beam expanders and the lenses of the microlens array, respectively.

As can be seen in Figure 1(b), each output channel is connected immediately behind the corresponding array component. The field

distribution of the outgoing beams is strongly influenced by that of the incident beam. Assume the field distribution of the incident beam to be a Gaussian profile, hence, the intensity of the individual outgoing beam can be determined by integrating the amplitude profile over a specific area covered by the corresponding array lens. Therefore, the equal-power output can be achieved by adjusting the apertures of the lenslets of the microlens array. As illustrated in Figure 1(b), each channel in the equal-power splitter is tapered approximately adiabatically into one of the eight single-mode output channels labeled 1 to 8. The apertures of channels 1 to 4 are 18.1 μm, 7.7 μm, 5.9 μm, and 4.3 μm, respectively.

The step and grid size in the BPM calculation is 1/20 of the wavelength and transparent boundary conditions are imposed in order to prevent reflection of the radiation waves at the boundaries of the calculation domain. The transmission efficiency is determined from the overlap integrals between the field calculated at the output position and the mode field of the input channel. The field distribution along the 1×8 equal-power splitter is plotted in Figure 2. The intensity distribution of the eight output channels is uniform and the total excess loss, which is defined as the total transmitted power divided by the incident power, is 0.28 dB. Figure 3 shows the distribution of output power on the eight output ports of the equal-power splitters. For demonstrating the effect of the lenslet aperture of microlens arrays, Figure 3 also shows the output-power distribution of the splitter with an equal lenslet aperture of 9 μm (the equal-aperture splitter). As can be seen, the output uniformity of the equal-power splitter is greatly uniform in comparison with the equal-aperture splitter. In the equal-power splitter, the output imbalance, which is defined as the maximum power divided by the minimum power, is 0.15 dB.

Since these lenses used the higher refractive indices, the propagation losses owing to reflection and scattering occur in the lens surfaces should be taken into account. However, the single-directional BPM is not suitable to simulate reflection and scattering in the boundaries between the waveguides and the lenses. Therefore, to evaluate the propagation losses that occur in the waveguide-lens boundaries, we use the FDTD method, which directly integrates Maxwell's equation in time, in order to calculate the transmission efficiency. The grid size used in the FDTD calculation is the same as that used in the BPM, and perfectly matched layer boundary conditions are implemented to avoid the reflection occurring in the

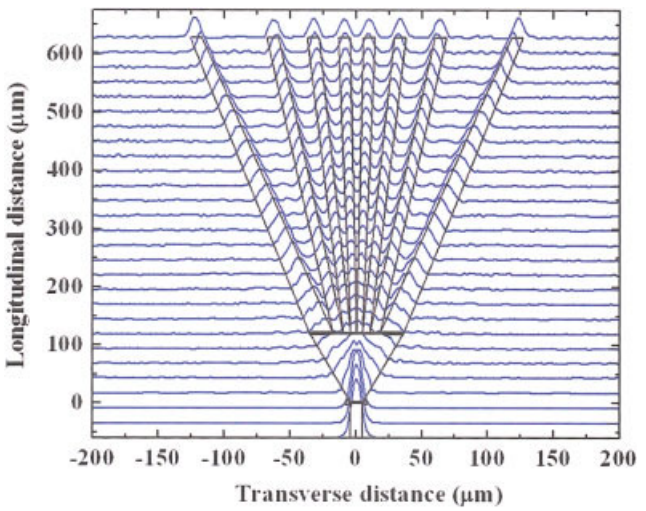

Figure 2 Plot of the field distribution along the equal-power splitter. [Color figure can be viewed in the online issue, which is available at www.interscience.wiley.com.]

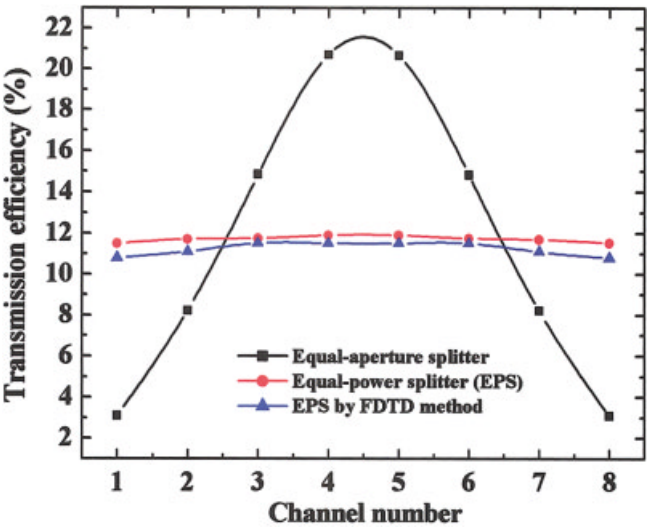

Figure 3 Distribution of output power on the eight output channels as a function of the channel number (channels 1 and 8 are the outermost output channels). [Color figure can be viewed in the online issue, which is available at www.interscience.wiley.com.]

boundaries of the calculation domain [15]. Figure 3 also shows that a total additional propagation loss of 0.19 dB is introduced by the reflection and scattering occurring in four waveguide-lens boundaries, and the calculated reflection loss is accordance with those obtained from the Fresnel's equation (about 0.14 dB). To evaluate the reflectance of the proposed equal-power splitter, the reflection wave is collected in the input waveguide in order to calculate the reflectance. Since the four waveguide-lens boundaries have curved surfaces, the reflection waves are either diverged or converged by the boundaries. Therefore, most reflection waves are not guided into the input channel, and the total reflectance in this device is -32.7 dB, which meets the requirement of -30 dB in a digital optical-fiber communication system. Additionally, as a result of wider incident angles, the propagation losses caused by the scattering and reflection in the waveguide-lens boundaries become larger in the outer channels of the equal-power splitter and the output imbalance grows to 0.3 dB. In addition, to show the functions of the beam expanders and the microlens arrays, the electric-field distribution obtained by the FDTD method is shown in Figure 4. For clear observation, the enlargements of the input and output portions of the tapered region are shown separately in Figures 4(a) and 4(b), respectively. As seen in Figure 4(a), the planar wavefronts of the input eigenmode launching from plane L were diverged by the beam expander and, as a result, more optical power was transformed to the outer region of the tapered

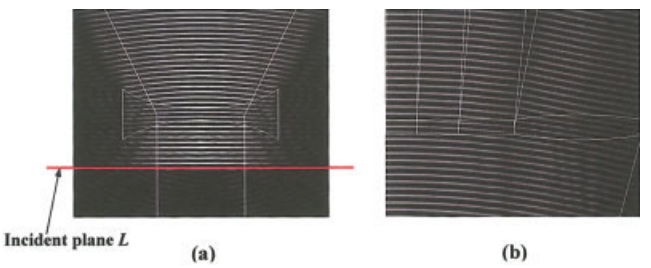

Figure 4 Electric-field distributions in the (a) input and (b) output channels of the equal-power splitter. [Color figure can be viewed in the online issue, which is available at www.interscience.wiley.com.]

waveguide. It can be found that the reflection and scattering waves appear in the waveguide-lens boundaries. Most reflected waves were radiated out and did not propagate backward along the input waveguide. Also, after passing through the microlens array in the output portion of the tapered waveguide, the curved wavefronts were flattened, so that the outgoing beams became plane-wave beams [see Fig. 4(b)].

A general fabrication issue of the radius deviation of lenses is discussed. In this analysis, the radius deviations of the beam expanders are assumed to be +5% and −5%, respectively. Figure 5 shows the distribution of output power on the eight output channels of the equal-power splitter with the parameters of the radius deviations. It is found that the output uniformity of the equal-power splitter was perturbed by the radius deviations of the beam expanders. As presented in Figure 5, since the +5% radius deviation of the beam expander would decrease the divergence angle in the tapered region, less power was transferred to the outer channels, which caused an apparent drop of output power in the outermost channels. Therefore, the excess losses were not affected by the +5% radius deviation; on the other hand, the output imbalance was raised to 0.77 dB. The −5% radius deviation of the beam expander redistributed the optical power in the tapered region; thus, the output imbalance was disturbed to 0.56 dB with an excess loss of 0.32 dB. As mentioned above, the ±5% radius deviation of the beam expander in the proposed equal-power splitters would cause the excess loss and output imbalance of 0.32 and 0.77 dB, respectively.

Spectral responses of power splitters are important issues in optical-fiber communications. For the purpose of evaluating the bandwidth of the proposed planar power splitters, the transmission efficiency is calculated as a function of wavelength from 1400 to 1600 nm. Figure 6 shows the output power of the eight output channels of the proposed equal-power splitter with different wavelengths. Due to dispersion of the guided-wave parameters, the output imbalance is proportional to the wavelength deviation. The output imbalance and the excess loss as a function of the wavelengths from 1400 to 1600 nm are shown in Figure 7. It is shown that the proposed device exhibits low excess losses across the wide spectral range from 1400 to 1600 nm, and the maximum excess

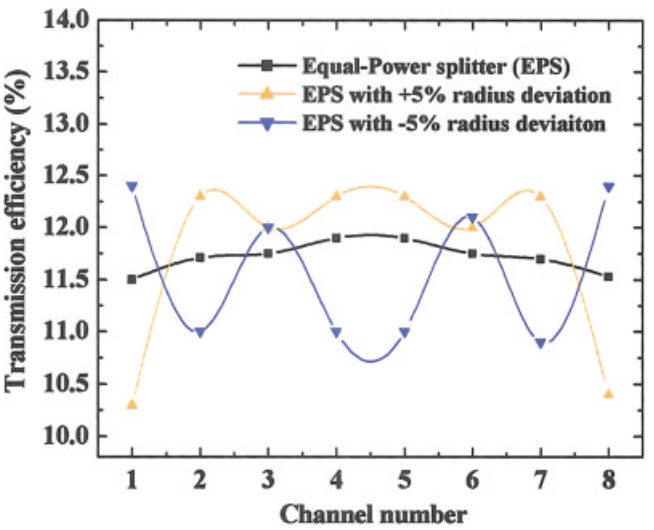

Figure 5 Distribution of output power on the eight output channels of the equal-power splitter with the parameters of the radius deviations. [Color figure can be viewed in the online issue, which is available at www.interscience.wiley.com.]

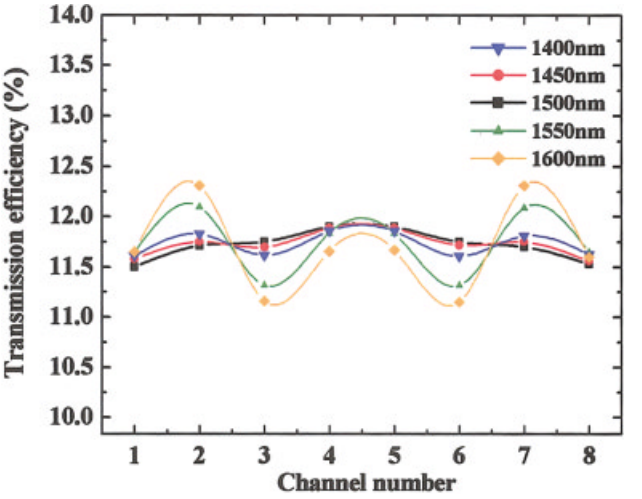

Figure 6 Distribution of output power on the eight output channels of the equal-power splitter with the parameters of the wavelength. [Color figure can be viewed in the online issue, which is available at www.interscience.wiley.com.]

loss in the analyzed spectral range is 0.29 dB. The output imbalance, on the other hand, is more sensitive to the operation wavelength. There is less uniformity in the long wavelengths than in the short wavelengths, and the maximum imbalance occurring at 1600 nm is 0.43 dB. Consequently, the proposed equal-power splitters exhibit a low excess loss of 0.29 dB and an acceptable output imbalance of 0.43 dB in the analyzed spectral ranges.

4. CONCLUSION

We have demonstrated compact 1 × 8 optical planar power splitters with low inherent losses of less than 0.28 dB using a guided-wave microlens array. The calculation results reveal that the bent angles of the output waveguides can be precisely determined by the proposed method, and low-loss and compact characteristics can be obtained successfully by the implementation of guided-wave lenses. By using the BPM and FDTD methods, the proposed equal-power splitters are analyzed to show low reflectance and acceptable fabrication tolerances in a wide range of operation wavelengths. Therefore, the guided-wave lens array is

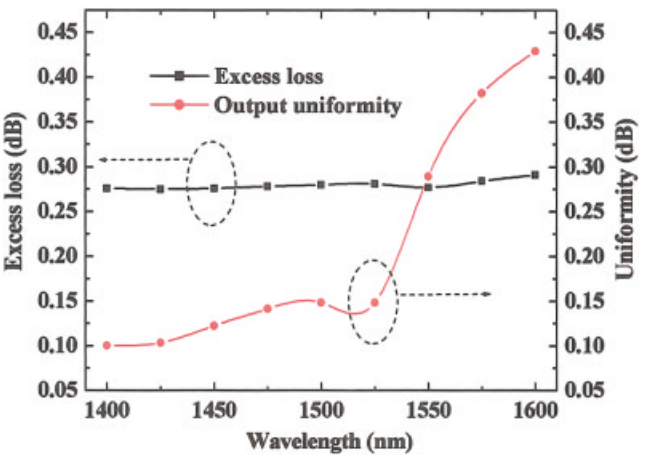

Figure 7 Wavelength responses of the proposed equal-power splitter. [Color figure can be viewed in the online issue, which is available at www.interscience.wiley.com.]

very useful for designing multibranch planar power splitters in broadband optical-communication systems.

ACKNOWLEDGMENT

This work was partially supported by the National Science Council of Taiwan under grant no. NSC-92-2112-M009-040.

REFERENCES

1. C. Chaudhari, D.S. Patil, and D.K. Gautam, A new technique for the reduction of the power loss in the Y-branch optical power splitter, Optics Commun 193 (2001), 121–125.
2. T. Yabu, M. Geshiro, and S. Sawa, New design method for low-loss Y-branch waveguides, J Lightwave Technol 19 (2001), 1376–1384.
3. W.Y. Hung, H.P. Chan, and P.S. Chung, Single-mode 1 × 3 integrated optical branching circuit design using phase-front accelerators, Electron Lett 24 (1988), 1365–1366.
4. T.J. Wang, Y.H. Wang, and W.S. Wang, Single-mode 1 × 3 equal-power divider using a substrate microprism and two waveguide expanders, IEEE Photon Technol Lett 12 (2000), 164–166.
5. C.C. Huang, C.Y. Chang, and W.S. Wang, Single-mode four-branch power divider with coupled wide-angle waveguides, Microwave Opt Technol Lett 38 (2003), 337–341.
6. J.A. Besley, J.D. Love, and W. Langer, A multimode planar power splitter, J Lightwave Technol 16 (1998), 678–684.
7. R.M. Jenkins, R.W. Devereux, and J.M. Heaton, Waveguide beam splitters and recombiners based on multimode propagation phenomena, Opt Lett 17 (1992), 991–993.
8. C. Themistos, B.M.A. Rahman, Design issues of a multimode interference-based 3-dB splitter, Appl Opt 41 (2001), 7037–7044.
9. T. Rasmussen, J.K. Rasmussen, and J.H. Povlsen, Design and performance evaluation of 1-by-64 multimode interference power splitter for optical communications, J Lightwave Technol 13 (1995), 2069–2074.
10. P.A. Besse, M. Bachmann, H. Melchior, L.B. Soldano, and M.K. Smit, Optical bandwidth and fabrication tolerances of multimode interference couplers, J Lightwave Technol 12 (1994), 1004–1009.
11. J. Park, Y. Chung, S. Baek, and H.-J. Lee, New design for low-loss star couplers and arrayed waveguide grating devices, IEEE Photon Technol Lett 14 (2002), 651–653.
12. M.M. Minot and C.C. Lee, A new guided-wave lens structure, J Lightwave Technol 8 (1990), 1856–1865.
13. C.W. Chang, M.L. Wu, and W.F. Hsieh, Design of low-loss tapered waveguides using the telescope structure compensation, IEEE Photon Technol Lett 15 (2003), 1378–1380.
14. K. Worhoff, A. Driessen, P.V. Lambeck, L.T.H. Hilderink, P.W.C. Linders, and T.J.A. Popma, Plasma enhanced chemical vapor deposition silicon oxynitride optimized for application in integrated optics, Sensors and Actuators 74 (1999), 9–12.
15. A. Taflove and S.C. Hagness, Computational electrodynamics: The finite-difference time-domain method for electromagnetics, Artech House, Boston, 2000.

COMPACT AND LOW-INSERTION-LOSS DUAL-MODE PATCH FILTER WITH SPUR-LINES

Y. Sung, B. Y. Kim, C. S. Ahn, and Y.-S. Kim
Korea University
Dept. of Radio Sciences Engineering
Seoul 136-701, Korea

Received 16 March 2004

ABSTRACT: *A compact microstrip dual-mode bandpass filter with inserted spur-lines at the edge of the patch is proposed. In order to obtain a low insertion loss, the proposed filter has no coupling gaps. Also, it has a size reduction of about 45% at the same resonant frequency as compared conventional dual-mode bandpass filters. Feed lines with offset are applied to ensure a minimal mismatch. From the measured results, the dual-mode filter has a 0.58-dB insertion loss at 1.27 GHz with 12% bandwidth.* © 2004 Wiley Periodicals, Inc. Microwave Opt Technol Lett 43: 33–34, 2004; Published online in Wiley InterScience (www.interscience.wiley.com). DOI 10.1002/mop.20366

Key words: *patch filter; dual-mode filter; spur-lines*

INTRODUCTION

A dual-mode planar resonator was proposed in the early 1970s by Wolff [1]. Dual-mode resonators have found widespread applications for satellite and wireless mobile-communication systems because they are characterized by small size, light weight, and low cost [2, 3]. An electrical coupling of two resonant modes generates a geometrical resonator, such as the ring resonator or the patch resonator. Modes that have the same resonant frequency are called degenerate modes. The field distributions of these two modes are orthogonal to each other. Coupling of the two modes is achieved by applying a small perturbation element along the orthogonal plane. The crucial aims are superior performance, small size, and low cost. Specially, low insertion loss, which is composed of conductor, dielectric, radiative, and coupling losses, is desirable for practical applications. Coupling loss, which is typically the dominant contributor among these losses, is dependent upon the coupling efficiency [2]. Generally, conventional patch resonators have two coupling gaps between the feed line and the patch resonator, and these coupling gaps affect the performance of the patch resonator. For a small gap, the coupling between the feed line and patch resonator is increased and the insertion loss of the patch resonator is reduced. However, the small size of a coupling gap gives rise to etching unreliability, which will affect the filter performance [3]. With only one coupling gap or without coupling gaps, the insertion loss of the patch resonator is lower than that of a conventional patch resonator with two coupling gaps [3, 4]. To provide the dual-mode band-pass filter with low insertion loss, we propose a novel configuration using a pair of spur-lines embedded in the patch (see Fig. 1). It is well known that the spur-line acts as a stop-band filter at some frequency bands [5]. In order to match the filter impedance well, 50Ω feed lines are shifted from the center of the square-patch resonator.

DUAL-MODE PATCH RESONATOR

The basic geometry of the microstrip-patch resonator investigated in this paper is shown in Figure 1. This filter consists of one square-patch resonator with a pair of orthogonal feed lines and two spur-lines. Without coupling gaps, 50Ω feed lines are directly connected to the patch resonator in order to obtain low insertion loss. The feed linewidth is chosen to have a characteristic impedance of 50Ω. The classical patch impedance-matching technique with offset d is adopted to ensure a good design with minimal mismatch. Both the patch and feed lines are located on a grounded dielectric substrate, which is characterized by relative permittivity $\varepsilon_r = 10.2$ and thickness $h = 1.27$ mm. The dimensions of the proposed structure are $L = 20$ mm and $W = 20$ mm, as shown in Figure 1. In order to facilitate the analysis, the feed lines have same offset at the input and output ports. It is found from the simulation that the resonant frequency shifts downward as the offset increases, while the peak points of the reflection coefficient S_{11} tends to go up slightly. The current flows in a counterclockwise direction, as illustrated in Figure 1. The signal path, which is from one side (input port) to the other (output port), is